European Journal of Mechanics / A Solids 115 (2026) 105842

Contents lists available at ScienceDirect

European Journal of Mechanics / A Solids

journal homepage: www.elsevier.com/locate/ejmsol

Full Length Article

Roton dispersion and displacement oscillatory for a nonlocal mechanical system

Ke Wang [a,b,*], Jonathan L.G. Schneider [b], Yi Chen [b,c], Julio Andrés Iglesias Martínez [b,c], Muamer Kadic [d], Changguo Wang [a,**]

[a] National Key Laboratory of Science and Technology on Advanced Composites in Special Environments, Harbin Institute of Technology, Harbin, 150001, China
[b] Institute of Applied Physics, Karlsruhe Institute of Technology (KIT), Karlsruhe, 76128, Germany
[c] Institute of Nanotechnology, Karlsruhe Institute of Technology (KIT), Karlsruhe, 76128, Germany
[d] Université de Franche-Comté, Institut FEMTO-ST, UMR 6174, CNRS, Besançon, 25000, France

ARTICLE INFO

Keywords:
Nonlocal metamaterials
Evanescent bloch modes
Frozen evanescent modes
Band structure
Spatial oscillation
Effective-medium approach
Higher-order differential equation

ABSTRACT

Recently, we revealed anomalous static response in metamaterials with strong beyond-nearest-neighbor interactions or nonlocal interactions. Therein, the displacement field of a metamaterial beam when stretched is not simply linear in space like for ordinary materials, but rather exhibits pronounced spatial oscillations. The unusual behavior originates from evanescent Bloch modes at zero frequency, or frozen evanescent modes, with large decaying length. Here, we start from a discrete nonlocal mass-and-spring model and adopt an effective-medium approach based on higher-order differential equation to describe the anomalous behaviors. We demonstrate that the theory well captures the frozen evanescent modes and predicates the exact spatial oscillations of the displacement field. The strong dependence of the displacement field on the beam length is also revealed. The feasibility of the effective-medium approach is validated by comparison with the uniaxial tensile test results of metamaterials designed to support the anomalous frozen evanescent phonons. This theory can potentially be used for exploring other intriguing phenomena in nonlocal materials.

1. Introduction

Metamaterials are often designed by engineering local interactions inside their unit cells (Kadic et al., 2019; Jiao et al., 2023; Krushynska et al., 2023; Chen et al., 2019; Karpov and Rahman, 2025; Han et al., 2025; Bergne et al., 2022), while nonlocal interactions between distant unit cells are less appreciated due to generally weak strength. Recent study shows that nonlocal interactions in metamaterials can be significantly enhanced and can even surpass local interactions by physically coupling non-neighboring unit cells (Chen et al., 2021; Fleury, 2021). Pronounced nonlocal interactions can drastically alter metamaterial dispersion bands and offer opportunity to shape any desired dispersion band (Kazemi et al., 2023). The highly unusual roton-like band, featured by a local minimum on the band at a finite wavenumber, is an interesting example (Cui et al., 2022; Zhu et al., 2022; Chen et al., 2023a; Duan et al., 2023; Rajabpoor Alisepahi et al., 2023; Yang et al., 2023; Samak and Bilal, 2024), which is previously only accessible in correlated quantum system (Landau, 1941; Godfrin et al., 2012). Such unusual band enables multiple interesting wave properties, e.g., negative refraction, multiple co-existing Bloch eigenstates (Wang et al., 2022).

Recent study further reveals that nonlocal mechanical systems not only exhibit exotic wave properties, but also show intriguing static response (Chen et al., 2024a). For an ordinary beam, unidirectional stretch leads to homogenous tension and a linear displacement field in the beam. In sharp contrast, local contraction and spatially-oscillating displacement field are possible in nonlocal metamaterial beams (Chen et al., 2024a). Furthermore, a longer beam can exhibit larger axial stiffness than a shorter beam. The counterintuitive response originates from the roton-like minimum induced zero-frequency evanescent mode at a finite complex-valued wavenumber (Chen et al., 2024a). The mode freezes in time due to zero frequency and is also called as frozen evanescent modes (Chen et al., 2024a; Martínez et al., 2025). Due to its

* Corresponding author. National Key Laboratory of Science and Technology on Advanced Composites in Special Environments, Harbin Institute of Technology, Harbin, 150001, China.
** Corresponding author. National Key Laboratory of Science and Technology on Advanced Composites in Special Environments, Harbin Institute of Technology, Harbin, 150001, China.
E-mail addresses: ke.wang2@partner.kit.edu (K. Wang), wangcg@hit.edu.cn (C. Wang).

https://doi.org/10.1016/j.euromechsol.2025.105842
Received 20 May 2025; Received in revised form 8 August 2025; Accepted 21 August 2025
Available online 30 August 2025

finite complex-valued wavenumber, k_{ZEM}, the mode exhibits a spatial oscillation period or "wavelength" of $p = 2\pi/|\mathrm{Re}(k_{ZEM})|$ and decays exponentially in space with a decaying length $l = 1/|\mathrm{Im}(k_{ZEM})|$. In general, frozen evanescent modes are ubiquitous in periodic systems. They are often negligible due to a small decaying length (Prodan, 2006). The roton-like minimum frequency can be brought sufficiently close to zero by engineering the nonlocal interactions, leading to anomalous frozen evanescent modes with much larger decaying length, which is essential for the unusual static response (Chen et al., 2024a).

Apart from the nonlocal interactions, different strategies, e.g., chirality, easy mode or mechanism mode, have been adopted for achieving roton-like bands (Kishine et al., 2020; Chen et al., 2024b; Bossart and Fleury, 2023; Groβ et al., 2024). We remark that the above unusual behavior is not limited to roton-like bands but can arise from general low-frequency minimums on dispersion band (Coulais et al., 2018). For mechanical metamaterials, a good strategy for achieving local minimums on dispersion bands is to adopt easy modes or zero modes in the design (Groβ et al., 2024), which are deformation modes that conceptually cost no strain energy. In fact, the frozen evanescent modes become easy modes when the local minimum exactly lies at zero (Chen et al., 2024a).

Though the physics of the unusual behaviors are well explained from frozen evanescent phonons (Chen et al., 2024a), this study does not incorporate an effective-medium continuum description, and the effective-medium continuum description of these modes remains elusive (Milton, 2002). Such continuum theory can potentially facilitate further optimization and application of the phenomenon without the demanding microstructure computation. Cauchy elasticity theory (Marin and Lesnic, 2004; Marin, 2009), which cannot account for nonlocal interactions, apparently is not suitable for the purpose. In literature, different continuum models have been proposed for nonlocal mechanical systems, including micropolar continuum theory, micromorphic elasticity, strain gradient elasticity and so on (Eringen, 1966; Shaat et al., 2020; Chen et al., 2020). Here, we specifically focus on discrete systems, which has been modeled previously by using fractional differential equations (Carpinteri et al., 2014) or high-order differential equations (Iglesias Martínez et al., 2021). The former is mainly considered when nonlocal interactions are relatively small and do not significantly change the dispersion bands (Chen et al., 2023b). The later has been derived for studying strong nonlocal interactions and has previously been used to study dynamic behaviors of nonlocal metamaterials (Chen et al., 2023b). Here, considering the nonlocal interactions of interest in our study, we adopt the later model for our purpose.

The paper is organized as below. We start from a one-dimensional mathematical toy model with strong nonlocal interactions based on masses and springs. A high-order differential equation description of the nonlocal model is also briefly introduced. Then, we compare frozen evanescent modes in the discrete model and an effective-medium model. We further study and compare the static response of a finite-length beam. Different parameters, including decaying length and system size, are studied. Finally, we compare the displacement field from the discrete model and the effective-medium model with the experimental results of the previously studied frozen evanescent phonon metamaterial. The results show that the effective-medium model can provide an excellent description of the observed unusual static response.

2. Nonlocal model and frozen evanescent modes

We first introduce the proposed infinite periodic nonlocal discrete mass-and-spring model with the lattice constant a shown in Fig. 1(a). The blue dots represent masses. The green zigzag lines represent springs, with spring constant K_1, and mediate local interactions between adjacent masses. The red lines stand for springs, with the spring constant K_3, between masses separated by a distance of $3a$. When the nonlocal interactions are sufficiently strong compared to the local interactions, the system will have a local minimum, or roton-like minimum, on its dispersion band, which can further lead to anomalous static effects.

From the Newton's equation of motion, the relationship between the acceleration $\ddot{u}_n$ and the displacement u_n at lattice site n can be expressed as follows

$$m\ddot{u}_n = K_1(u_{n+1} - 2u_n + u_{n-1}) + K_3(u_{n+3} - 2u_n + u_{n-3}). \tag{1}$$

In order to obtain the dispersion relation, we assume the Bloch wave ansatz, $u_n(t) = \tilde{u}\exp(\mathrm{i}(nka - \omega t))$, where $\tilde{u}$ represents the amplitude, i denotes the imaginary part, ω and k, are the frequency and wavenumber, respectively. By applying the Bloch wave ansatz to Eq. (1), the dispersion relation is obtained

$$\omega(k) = 2\sqrt{\frac{K_1}{m}\sin^2\left(\frac{ka}{2}\right) + \frac{K_3}{m}\sin^2\left(\frac{3ka}{2}\right)} \tag{2}$$

A roton-like band is obtained when $K_3/K_1 > 1/3$ (Chen et al., 2021), as illustrated in Fig. 2. A local minimum frequency $\omega_{\min}$ occurs at a finite wavenumber $k_{\min}$. Previous investigations have elucidated that the emergence of the minimum on the roton-like band stems from extraordinary Bragg reflection interactions, arising from the intricate interplay between local interactions and nonlocal interactions. The slope of the dispersion relation in the long-wavelength limit is c_0. These parameters can be derived from the dispersion relation in Eq. (2) and are given

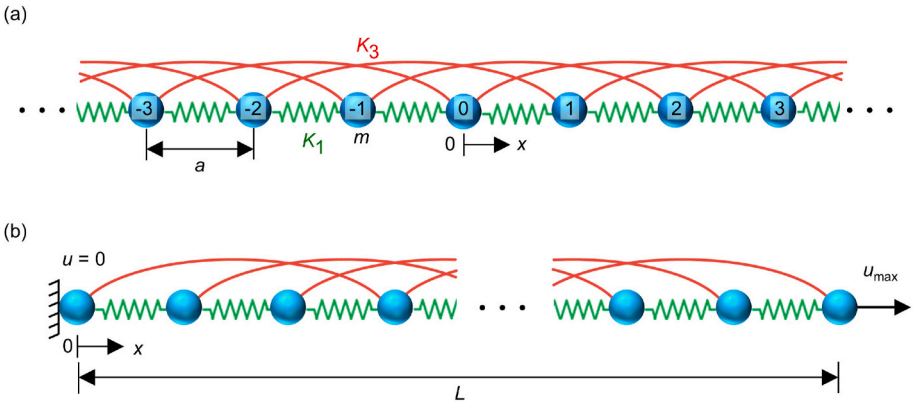

Fig. 1. One-dimensional nonlocal mass-and-spring model. (a) Infinite mass-and-spring model with nearest-neighbor and third-nearest-neighbor interactions. Masses m are represented by blue dots. The green zigzag lines represent the nearest-neighbor springs with spring constant K_1. The red lines correspond to the third-nearest-neighbor springs with spring constant is K_3. We number each mass and select the central mass as the origin of the coordinates. (b) A finite system with length L.The left-hand side is fixed and a displacement constraint is applied to the right-hand side. (For interpretation of the references to colour in this figure legend, the reader is referred to the Web version of this article.)

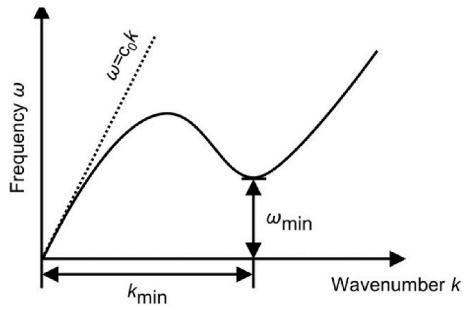

Fig. 2. Schematic diagram of a roton-like dispersion relation. The parameter c_0 represents the slope of the roton-like dispersion relation in the long wavelength limit. $\omega_{\min}$ is the local minimum frequency at a finite wavenumber $k_{\min}$.

below

$$\begin{cases} c_0 = \sqrt{\dfrac{K_1 + 9K_3}{m}} \\ k_{\min} = 2\,\mathrm{atan}\left(\sqrt{\dfrac{6+\sqrt{9-3K_1/K_3}}{6-\sqrt{9-3K_1/K_3}}}\right) \\ \omega_{\min} = \sqrt{\dfrac{K_1}{3m}}\sqrt{6+2\sqrt{1-K_1/(3K_3)}+6K_3\Big/K_1-K_3\Big/K_1\sqrt{(9-3K_1/K_3)}} \end{cases} \tag{3}$$

In order to describe the nonlocal mass-and-spring model with an effective-medium approach, we first need to obtain a continuum version of the governing Eq. (1). This can be done by replacing the finite difference operators with ordinary differential operators (Chen et al., 2023b). Considering the balance between computational efficiency and accuracy, we chose to use up to the sixth order derivatives in this study, which is a minimal continuum model to reproduce the roton-like minimum. For example, a truncation to second-order derivatives leads to a monotonic dispersion relation, while a truncation to fourth-order only captures a local maximum on the dispersion relation but not the local minimum. The inclusion of even higher-order derivatives, such as eight-order derivatives, can provide similar quantitative agreement (Fig. S4–S7 in Supplementary Material) between the continuum model and the discrete system, however, it requires more intricate boundary conditions. By truncating to six-order spatial derivative, the following governing equation is derived (Chen et al., 2023b)

$$\frac{\partial^2 u(x,t)}{\partial t^2} = A_2\frac{\partial^2 u(x,t)}{\partial x^2} + A_4\frac{\partial^4 u(x,t)}{\partial x^4} + A_6\frac{\partial^6 u(x,t)}{\partial x^6}. \tag{4}$$

Here, A_2, A_4 and A_6 are unknown material parameters and $u(x,t)$ is the displacement field. With the plane wave ansatz, we can derive the following dispersion relation

$$\omega(k) = \sqrt{\left(A_2k^2 - A_4k^4 + A_6k^6\right)} \tag{5}$$

The material parameters A_2, A_4 and A_6 can be obtained by fitting Eq. (5) to the dispersion relation of the discrete model, i.e., Eq. (2). Specifically, we match the slope of the dispersion relation in the long-wavelength limit, the wavenumber, $k_{\min}$, and the frequency, $\omega_{\min}$, for the roton-like minimum. The three material parameters can then be obtained from c_0, $\omega_{\min}$ and $k_{\min}$, introduced in Eq. (3),

$$\begin{cases} A_2 = c_0^2 \\ A_4 = \left(2c_0^2k_{\min}^2 - 3\omega_{\min}^2\right)/k_{\min}^4 \\ A_6 = \left(c_0^2k_{\min}^2 - 2\omega_{\min}^2\right)/k_{\min}^6 \end{cases} \tag{6}$$

The obtained material parameters in Eq. (6) are used for the following comparison between the discrete model and the continuum theory. The coefficients in Eq. (6) are expressed in terms of the three parameters c_0, $\omega_{\min}$ and $k_{\min}$, which are related to K_1 and K_3. In principle, the three coefficients A_2, A_4 and A_6 can be explicitly formulated as functions of K_1 and K_3. However, such expressions are excessively lengthy and cumbersome. To maintain clarity and conciseness, the coefficients in Eq. (6) are instead expressed in terms of the intermediate parameters c_0, $\omega_{\min}$ and $k_{\min}$.

We first compare the dispersion relation and the frozen evanescent phonons from the two calculations. In Fig. 3(a), we plot the dispersion relation of the discrete system (dashed lines) and the continuum model (solid lines) for a stiffness ratio $K_3/K_1 = 30$. The roton-like dispersion relations (black dashed and solid lines) are given in the grey plane. Two branches (yellow and green branches) with complex-valued wavenumber start from the roton-like minimum and arrive at the $\omega = 0$ plane. The highlighted yellow dots and green dots correspond to frozen evanescent phonons (Chen et al., 2024a). They constitute part of the solutions for static response of a finite system and are essential for the following observed anomalous effects. The displacement fields of the frozen evanescent phonons are plotted in Fig. 3(b). They have an oscillation period of $\lambda = 2\pi/\mathrm{Re}(k) \approx 3a$ and exponentially decays in space. The decaying direction is determined by the sign of the imaginary part of its wavenumber. A positive imaginary component indicates exponentially decaying towards the right (see yellow lines and dots in (b)). Likewise, a negative imaginary component means exponentially decaying towards the left (see green lines and dots in (b)). We obtain a nice agreement between the discrete model and the continuum theory. Smaller stiffness ratio leads to frozen evanescent phonons with much smaller decaying length (see Supplementary Material Fig. S1–S3).

3. Anomalous static response

Herein, we consider a finite beam system with length L as depicted in Fig. 1(b). The system is fixed at the left end and a displacement load $u_{\max}$ is applied to the right-hand side. In an ordinary mass-and-spring system with only local interactions, a static stretch leads to a linear displacement field of the system. However, the situation becomes rather different here for the nonlocal system with frozen evanescent phonon modes. The force-balance equation for the mass at lattice site n writes as (Chen et al., 2024a)

$$K_1(u_{n+1} + u_{n-1} - 2u_n) + K_3(u_{n+3} - 2u_n + u_{n-3}) = 0, n = 3, \ldots L/a - 3. \tag{7}$$

The total displacement field is the superposition of several parts. First, the following linear or affine displacement field must be involved as it apparently satisfies the above Eq. (7)

$$u_n^{\mathrm{affine}} = E_5 + E_6 n, n = 0, 1, 2\ldots, L/a, \tag{8}$$

with E_5 and E_6 being unknown constants. Furthermore, multiple frozen evanescent phonon solutions of the following form must be included

$$u_n^{\mathrm{FEP}} = \exp\left(\mathrm{i}k_j(na - L/2)\right), n = 0, 1, 2\ldots, L/a. \tag{9}$$

In which, k_j must satisfy the same dispersion relation as in Eq. (2)

$$K_1\sin^2\left(\frac{k_ja}{2}\right) + K_3\sin^2\left(3\frac{k_ja}{2}\right) = 0 \tag{10}$$

We only need consider solutions of k_j with its real part inside the first Brillouin zone, $-\pi/a < \mathrm{Re}(k_j) \le \pi/a$. Other solutions of k_j is simply translation of integer multiples of $2\pi/a$, which does not affect the displacement field solution of frozen evanescent phonons in Eq. (9).

In Fig. 3(a), we only plot the dispersion relations with $\mathrm{Re}(k) > 0$. In fact, the dispersion relation exhibits mirror symmetry with respect to the plane of $\mathrm{Re}(k) = 0$. For the mass-and-spring model, with these parameters used in Fig. 3(a), we obtain frozen evanescent phonons with the

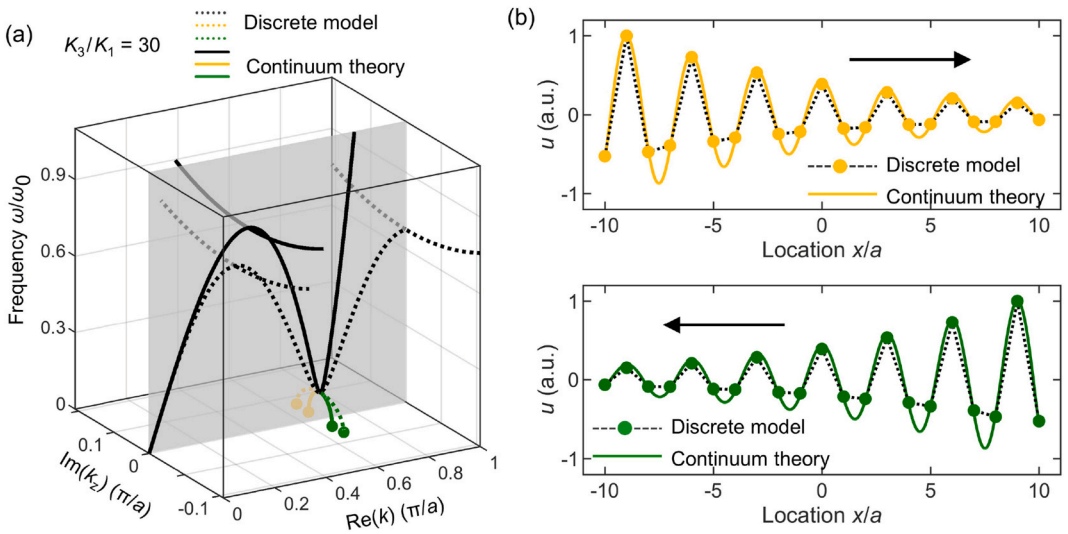

Fig. 3. Dispersion relation in complex-valued wavenumber space and frozen evanescent phonons. (a) Dispersion relations for the discrete model (dashed lines) and the continuum model (solid lines). The stiffness ratio is $K_3/K_1 = 30$. The curves on the grey plane are the dispersion relations for real wavenumbers and roton-like minimums are clearly seen. Two complex dispersion branches with real frequency but complex-valued wavenumbers emerge from the roton-like minimum and reach down to the $\omega = 0$ plane, leading to frozen evanescent phonons (see the yellow and green dots) at wavenumbers $k_z \approx (0.666 \pm 0.033\,\mathrm{i})\,\pi/a$ for the discrete model and at wavenumbers $k_z \approx (0.666 \pm 0.017\,\mathrm{i})\,\pi/a$ for the continuum model. (b) Illustration of the displacement field of the frozen evanescent phonons localized at left end (cf. yellow dots) and localized at right end (cf. green dots). Results for $K_3/K_1 = 15$, $K_3/K_1 = 5$ and $K_3/K_1 = 1$ are shown in Supplementary Material Fig. S1–S3. (For interpretation of the references to colour in this figure legend, the reader is referred to the Web version of this article.)

below wavenumbers

$$k_1 = (0.666 + 0.033\mathrm{i})\pi/a, k_2 = (-0.666 + 0.033\mathrm{i})\pi/a, k_3 = -k_1, k_4 = -k_2. \tag{11}$$

As stated before, the decaying direction of the displacement field in Eq. (9) is related to the imaginary part of the wavenumber k_j.

The total displacement field of the mass-and-spring model can be assumed to be a linear combination of the above several parts

$$u_n = E_5 + E_6 n + \sum_{j=1}^{j=4} E_j \exp(\mathrm{i}k_j n a) \tag{12}$$

The total displacement field Eq. (12) automatically ensure the force-balance condition in Eq. (7). The unknown coefficients E_0, E_1 and E_j depends on the boundary conditions. Specifically, the first and the last masses are prescribed with known displacement

$$u_0 = 0, u_{L/a} = u_{\max}. \tag{13}$$

Furthermore, the masses at lattice sites 1, 2, $L/a - 2$ and $L/\ a-\ 1$ must be balanced

$$\begin{cases} K_1(u_0 + u_2 - 2u_1) + K_3(u_4 - u_1) = 0 \\ K_1(u_1 + u_3 - 2u_2) + K_3(u_5 - u_2) = 0 \\ K_1(u_{L/a-3} + u_{L/a-1} - 2u_{L/a-2}) + K_3(u_{L/a-5} - u_{L/a-2}) = 0 \\ K_1(u_{L/a-2} + u_{L/a} - 2u_{L/a-1}) + K_3(u_{L/a-4} - u_{L/a-1}) = 0 \end{cases} \tag{14}$$

From the above six conditions in Eqs. 13 and 14, the six unknown coefficients $E_1, \ldots E_6$ can be determined. The total displacement field and different parts are therefore obtained.

Next, we solve the displacement field of the finite length beam by using the continuum model as demonstrated previously. The displacement field satisfy a similar differential equation as in Eq. (4)

$$A_2 \frac{\partial^2 u(x)}{\partial x^2} + A_4 \frac{\partial^4 u(x)}{\partial x^4} + A_6 \frac{\partial^6 u(x)}{\partial x^6} = 0. \tag{15}$$

Here, the displacement field $u(x)$ is time independent. The minimal spatial derivative in Eq. (15) is second order, therefore the following affine solution must be one part of the total displacement field

$$u^{\mathrm{affine}}(x) = C_5 x + C_6, \tag{16}$$

C_5 and C_6 are two unknown coefficients. In addition, the continuum model exhibits similar frozen evanescent phonons as in the discrete system. We can assume the following displacement form

$$u^{\mathrm{FEP}}(x) = \exp(\mathrm{i}kx). \tag{17}$$

In which, the parameter k satisfy

$$k^2(A_2 - A_4 k^2 + A_6 k^4) = 0 \tag{18}$$

The solution of $k = 0$ actually corresponds to the linear solution in Eq. (16). We only need to consider non zero solutions of k

$$k_1 = \sqrt{\frac{A_4 - \sqrt{A_4^2 - 4A_6A_2}}{2A_6}}, k_2 = -k_1, k_3 = \sqrt{\frac{A_4 + \sqrt{A_4^2 - 4A_6A_2}}{2A_6}}, k_4 = -k_3. \tag{19}$$

The total displacement field can then be assumed as a linear combination of the above solutions

$$u(x) = C_5 x + C_6 + \sum_{j=1}^{j=4} C_j \exp(\mathrm{i}k_j x). \tag{20}$$

The six unknown coefficients C_1, C_2, C_3, C_4, C_5 and C_6 need to be determined from the boundary conditions. However, the formulation of boundary conditions in nonlocal continuum models remains a subtle issue, especially for boundaries where artificial constraints may arise. This challenge has been extensively discussed in the literature (Ceballes et al., 2021; Puglisi, 2006, 2007), including the work by Ceballes et al. (2021), which highlights several paradoxes and inconsistencies associated with nonlocal boundary treatments. In this study, the boundary conditions have been carefully selected to reflect the physics and also to ensure a nice agreement between the discrete model and the continuum model. Specifically, the following set of boundary conditions is applied:

$$\begin{cases} u|_{x=0} = 0, u|_{x=L} = u_{\max} \\ \frac{\partial u}{\partial x}|_{x=0} + \frac{\partial u}{\partial x}|_{x=L} = 0, \frac{\partial^2 u}{\partial x^2}|_{x=0} + \frac{\partial^2 u}{\partial x^2}|_{x=L} = 0 \\ \frac{\partial^3 u}{\partial x^3}|_{x=0} + \frac{\partial^3 u}{\partial x^3}|_{x=L} = 0, \frac{\partial^4 u}{\partial x^4}|_{x=0} + \frac{\partial^4 u}{\partial x^4}|_{x=L} = 0 \end{cases} . \tag{21}$$

The first two equations correspond to the clamped and loaded displacement boundaries at the left and right end of the beam, respectively. The remaining four boundary conditions impose anti-symmetric conditions to the derivatives of the displacement field at the two ends of the beam. In general, displacement derivatives, such as the first-order derivative, are related to forces or gradients of forces if nonlocal interactions are included. As a result, the four equations ensure that the forces and gradients of forces at the two boundaries are balanced. This set of boundary conditions is also compatible with the symmetry of the 1D discrete model with respect to its middle point. As will be demonstrate later, the adopted boundaries here capture the essential physical response.

Now, we compare the obtained displacement fields of the stretched finite length beam by using the discrete model and the continuum theory. Fig. 4(a) illustrates the total displacement field with stiffness ratio $K_3/K_1 = 30$ and length $L = 29a$. Unlike the linear displacement field of an ordinary mass-and-spring model with only local interactions, the displacement field for the nonlocal mode here exhibits pronounced spatial oscillations with period of $3a$. The dashed line with blue dots represents the discrete mass-and-spring model, and the solid line depicts the effective-medium results. The result from the continuum model (see black line) is in perfect agreement with the discrete model calculations (see blue dots), indicating that the derived continuum theory can adequately describe the discrete mass-and-spring system.

We show in Fig. 4(b) the decomposed displacement field as introduced in the previous analysis. This clearly demonstrates that the observed oscillations in the total displacement field arise from the frozen evanescent phonons localized at both ends of the finite system. It is interesting to note that the two frozen evanescent phonons can interfere, just like waves, albeit the analysis here is purely static. For examples, for a beam length commensurate to the frozen evanescent phonon wavelength (see panels (c) and (d)), the two frozen evanescent phonons are exactly out-of-phase. This phenomenon highlights the destructive interference between the two solutions, resulting in attenuated spatial oscillations in the central region (see the grey area in panel (c)). Conversely, constructive interference gives rise to amplified oscillations in the central region (see the grey area in panel (a)). It is worth noting that this pronounced sensitivity of the displacement field to the system length is absent in ordinary local systems.

The stiffness ratio K_3/K_1 is an important factor that influences the decaying length of the frozen evanescent phonons (see Supplementary Material Fig. S1–S3). For smaller K_3/K_1, the total displacement field exhibits much less spatial oscillation and gradually approaches a simply linear field as in an ordinary material (see Fig. 5), in consistent with the much smaller decaying length of the frozen evanescent phonons (see Supplementary Material Fig. S1–S3). Here, we also obtain nice agreement between the discrete model and the continuum theory.

4. Comparison with experiments

To further validate the proposed effective-medium continuum model, we compare its predictions with our previous experiments on nonlocal metamaterial beams (Chen et al., 2024a). For completeness and readability, we show in Fig. 6 our previously designed and

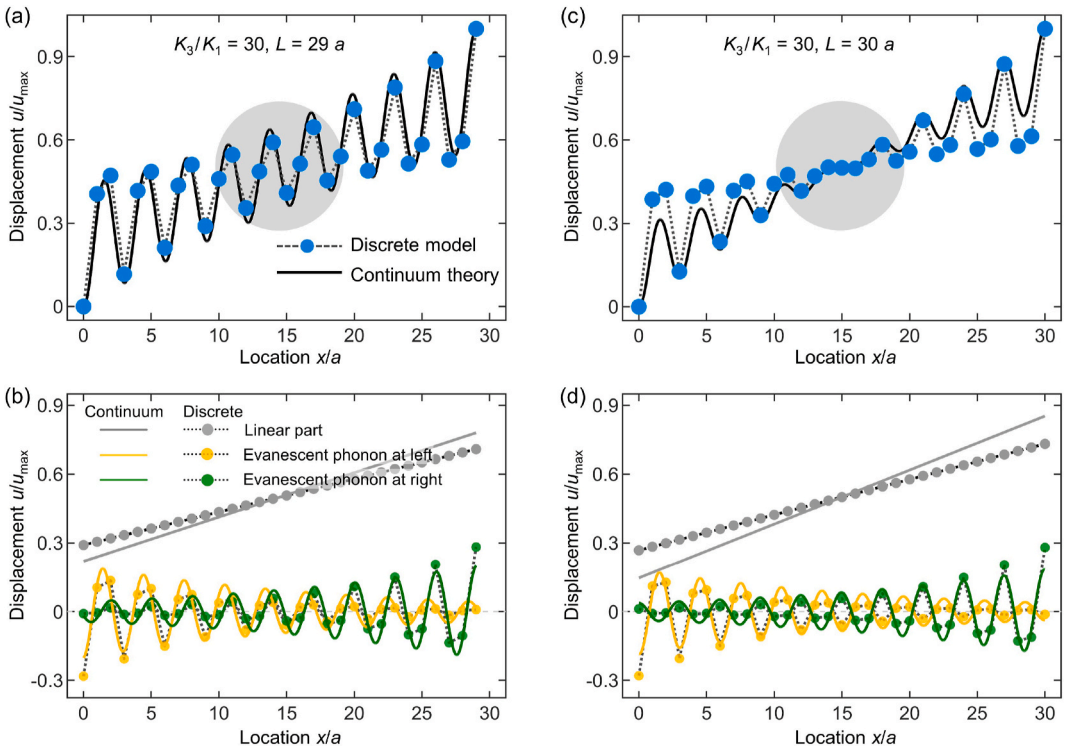

Fig. 4. Anomalous displacement field of a finite nonlocal system under stretching. (a) Comparison between the displacement field of the mass-and-spring model (blue dots) and the effective-medium model (black line) for $K_3/K_1 = 30$. The length of the system is $L = 29a$. (b) Decomposition of the total displacement field. The total displacement comprises three components: a linear part (cf. grey line), a frozen evanescent phonon localized at left end (cf. yellow curve), and a frozen evanescent phonon localized at right end (cf. green curve). The two frozen evanescent phonons manifest in-phase displacement, leading to constructive interference. (c) and (d) Same as (a) and (b) but for length $L = 30a$. The middle region has a much smaller oscillation magnitude (cf. blue dots in the grey region), resulting from destructive interference between the two frozen evanescent phonons. (For interpretation of the references to colour in this figure legend, the reader is referred to the Web version of this article.)

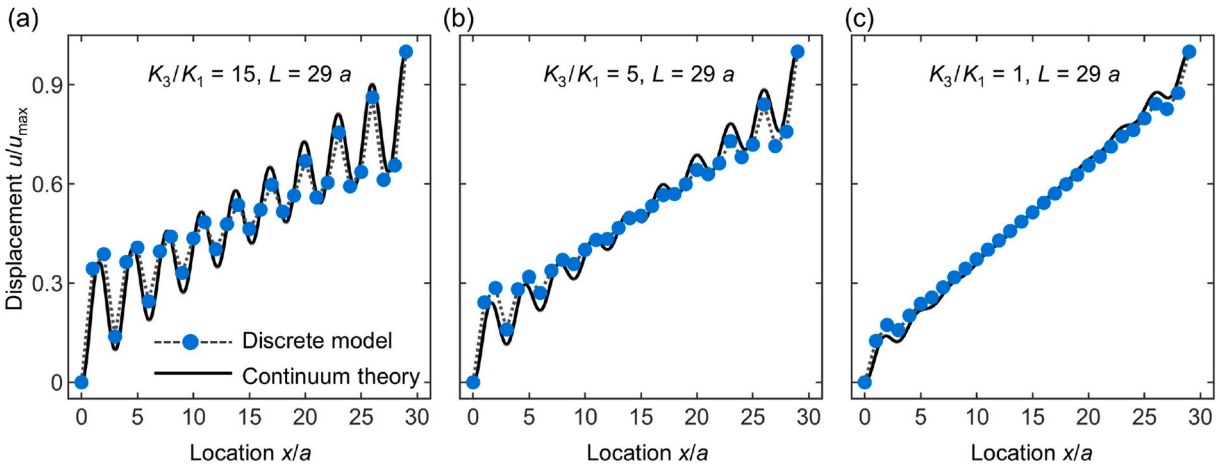

Fig. 5. Displacement field of a finite nonlocal system under stretching as in Fig. 4(a) but for (a) $\boldsymbol{K_3/K_1 = 15}$, (a) $\boldsymbol{K_3/K_1 = 5}$, (c) $\boldsymbol{K_3/K_1 = 1}$.

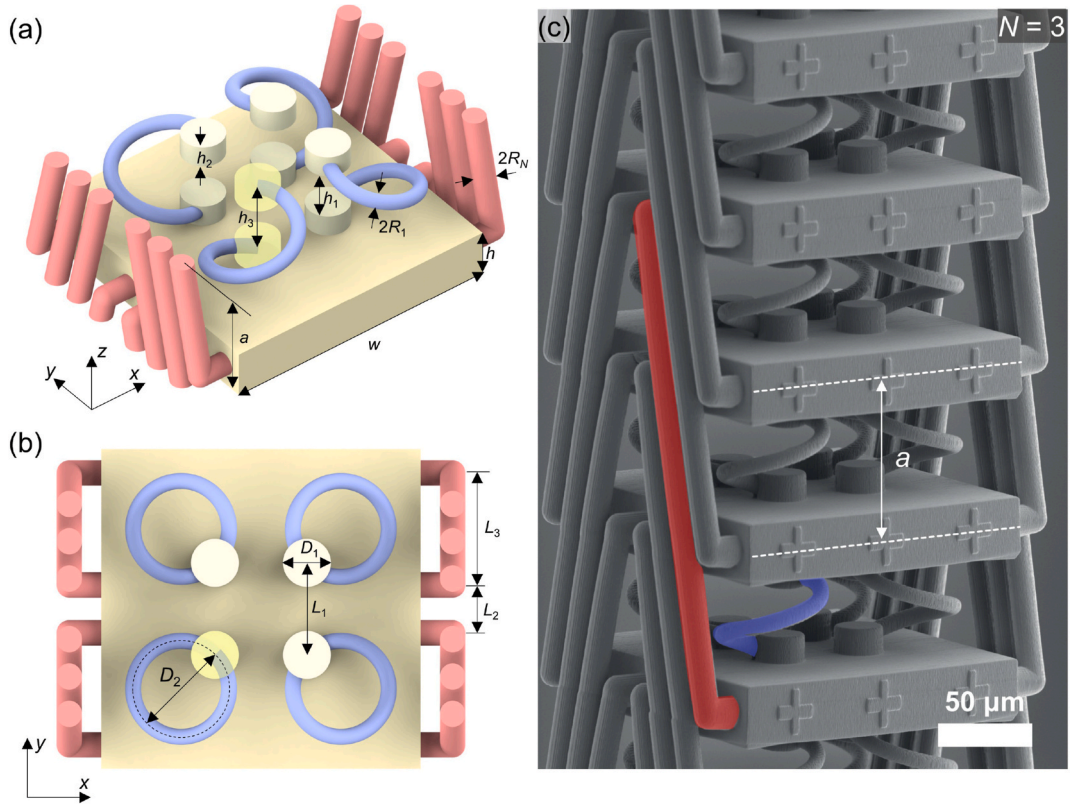

Fig. 6. Schematic of the metamaterial structure enabling anomalous frozen evanescent phonons in literature (Chen et al., 2024a)**.** (a) The side view of the metamaterial unit cell. (b) The top view of the metamaterial unit cell. (c) The scanning-electron micrograph (SEM) image of the metamaterial, with nearest-neighbor (blue) and third-nearest-neighbor (red) interactions highlighted. Adapted with permission from Ref. (Chen et al., 2024a), Copyright © 2024, Yi Chen et al. (For interpretation of the references to colour in this figure legend, the reader is referred to the Web version of this article.)

fabricated metamaterial, adopted from Ref. (Chen et al., 2024a). The yellow plates in Fig. 6(a) and (b) represent masses. The blue helices represent the nearest-neighbor connections between the masses, while red rods indicate third-nearest-neighbor interactions. A scanning-electron micrograph (SEM) is presented in Fig. 6(c). A direct mapping of the metamaterial structure onto a discrete mass-and-spring model leads to our system in Fig. 1(a).

We compare in Fig. 7 the calculated displacement fields with previous experiment results for different beam lengths ($L = 38a, 39a$ and $40a$). The experimental results (dashed line with red dots) in Fig. 7 are reproduced from our previous work (Chen et al., 2024a). The displacement field shown in Fig. 7 exhibit oscillatory behavior that varies with the system length, which is distinct from the linear displacement fields typically observed in conventional materials. Overall, we observe excellent agreement between results from our continuum model (black solid lines), discrete model (blue dotted lines) and the experimental results (dashed line with red dots). When the system length is commensurate with the nonlocal interaction order ($N = 3$) (see Fig. 7(b)), the oscillation amplitude near the center is much smaller compared to non-commensurate cases (see Fig. 7(a) and (c)). As discussed in the preceding analysis, this phenomenon occurs because the evanescent Bloch wave modes excited from the left and right sides are

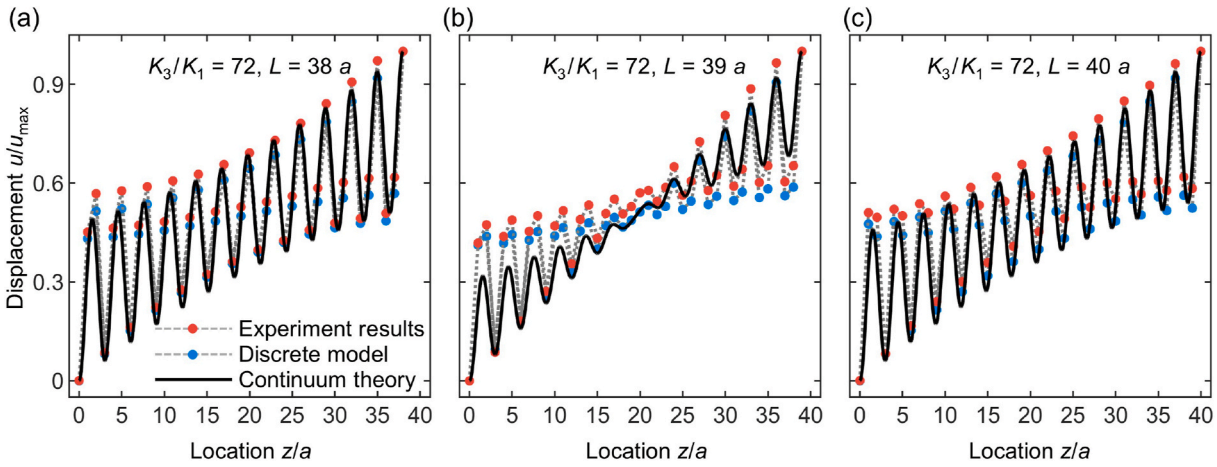

Fig. 7. The oscillatory displacement field of the stretched metamaterial beam with different lengths. (a) $K_3/K_1 = 72, L = 38a$. (b) $K_3/K_1 = 72, L = 39a$. (c) $K_3/K_1 = 72, L = 40a$. The red dotted line represent the experimental measurements (reproduced with permission from Ref. (Chen et al., 2024a), Copyright © 2024, Yi Chen et al.), the blue dotted line correspond to the mass-and-spring model, the black solid line denotes the continuum model. (For interpretation of the references to colour in this figure legend, the reader is referred to the Web version of this article.)

out of phase, resulting in destructive interference at the center and consequently leading to a diminished oscillation amplitude. A comparison of the three configurations in Fig. 7 clearly shows that adding or removing a single unit cell can lead to significant changes in the displacement field. This sensitivity to structural length suggests potential applications in the design of remote mechanical sensing devices.

We note that the studied anomalous static effects, including oscillatory displacement field and size effects, are not limited to systems with the specific third-order nonlocal interactions. Other nonlocal interactions generally could also lead to similar effects if they can induce dispersion relations with similar roton-like minima. For instances, chirality and delocalized zero modes have been introduced to achieve roton-like dispersion relations in metamaterials (Chen et al., 2024b; Groβ et al., 2024), though the corresponding static effects have not been demonstrated. Moreover, nonlocal interactions that decay exponentially or algebraically with distance (Puglisi, 2006, 2007) could potentially lead to analogous static responses. These alternatives represent promising directions for future investigation. We briefly remark that similar unusual static effects have already been numerically studied in two-dimensional systems (Chen et al., 2024a) and are expected to occur in three-dimensional architectures as well.

5. Conclusion

We presented an effective-medium approach to describe the anomalous static response of a nonlocal metamaterial. The theory is based on a higher-order differential equation, with spatial derivatives up to six-order. We obtained a satisfying agreement between the effective-medium calculations and a proposed nonlocal mass-and-spring model at different levels, including the slow-decaying frozen evanescent modes, the oscillatory displacement profile of a stretched beam, and its strong dependence of the displacement response to the beam length. The consistency with experiment validation further confirms the reliability of this effective-medium approach. We anticipate that this study will stimulate other investigations into anomalous static responses in mechanical metamaterials. Furthermore, similar anomalous static effects may not be limited to mechanical field but can be generalized to other physical areas. This oscillating displacement field is expected to be used in areas such as signal detection in the future.

Declaration of competing interest

All authors declare no conflict of interest.

CRediT authorship contribution statement

Ke Wang: Writing – original draft, Visualization, Validation, Software, Resources, Formal analysis, Data curation, Conceptualization. **Jonathan L.G. Schneider:** Visualization, Validation, Methodology, Data curation. **Yi Chen:** Writing – original draft, Supervision, Project administration, Investigation, Formal analysis, Conceptualization. **Julio Andrés Iglesias Martínez:** Validation, Investigation, Formal analysis, Data curation. **Muamer Kadic:** Supervision, Software, Resources, Data curation. **Changguo Wang:** Writing – review & editing, Supervision, Resources, Funding acquisition.

Declaration of competing interest

The authors declare that they have no known competing financial interests or personal relationships that could have appeared to influence the work reported in this paper.

Acknowledgements

We acknowledge Prof. Martin Wegener (KIT) for inspiring discussions. C.W. is grateful for support by the National Natural Science Foundation of China (contract 12172102). This research has been funded by the Deutsche Forschungsgemeinschaft (DFG, German Research Foundation) under Germany's Excellence Strategy via the Excellence Cluster "3D Matter Made to Order" (EXC-2082/1–390761711). K.W. is supported by the China Scholarship Council (K.W.). M.K. acknowledges support by the EIPHI Graduate School (contract ANR-17-EURE-0002).

Appendix A. Supplementary data

Supplementary data to this article can be found online at https://doi.org/10.1016/j.euromechsol.2025.105842.

Data availability

Data will be made available on request.

References

Bergne, A., Baardink, G., Loukaides, E.G., Souslov, A., 2022. Scalable 3D printing for topological mechanical metamaterials. Extreme Mechanics Letters 57, 101911.
Bossart, A., Fleury, R., 2023. Extreme spatial dispersion in nonlocally resonant elastic metamaterials. Phys. Rev. Lett. 130 (20), 207201.

Carpinteri, A., Cornetti, P., Sapora, A., 2014. Nonlocal elasticity: an approach based on fractional calculus. Meccanica 49 (11), 2551–2569.
Ceballes, S., Larkin, K., Rojas, E., Ghaffari, S.S., Abdelkefi, A., 2021. Nonlocal elasticity and boundary condition paradoxes: a review. J Nanopart Res 23 (3), 66.
Chen, Y., Liu, X., Hu, G., 2019. Topological phase transition in mechanical honeycomb lattice. J. Mech. Phys. Solid. 122, 54–68.
Chen, Y., Frenzel, T., Guenneau, S., Kadic, M., Wegener, M., 2020. Mapping acoustical activity in 3D chiral mechanical metamaterials onto micropolar continuum elasticity. J. Mech. Phys. Solid. 137, 103877.
Chen, Y., Kadic, M., Wegener, M., 2021. Roton-like acoustical dispersion relations in 3D metamaterials. Nat. Commun. 12 (1), 3278.
Chen, Y., Abouelatta, M.A.A., Wang, K., Kadic, M., Wegener, M., 2023a. Nonlocal cable-network metamaterials. Adv. Mater. 35 (15), 2209988.
Chen, Y., Wang, K., Kadic, M., Guenneau, S., Wang, C.G., Wegener, M., 2023b. Phonon transmission through a nonlocal metamaterial slab. Commun. Phys. 6 (1), 1–11.
Chen, Y., Schneider, J.L.G., Wang, K., Scott, P., Kalt, S., Kadic, M., Wegener, M., 2024a. Anomalous frozen evanescent phonons. Nat. Commun. 15 (1), 8882.
Chen, Y., Schneider, J.L.G., Groß, M.F., Wang, K., Kalt, S., Scott, P., Kadic, M., Wegener, M., 2024b. Observation of chirality-induced roton-like dispersion in a 3D micropolar elastic metamaterial. Adv. Funct. Mater. 34 (20), 2302699.
Coulais, C., Kettenis, C., van Hecke, M., 2018. A characteristic length scale causes anomalous size effects and boundary programmability in mechanical metamaterials. Nature Phys 14 (1), 40–44.
Cui, J.G., Yang, T., Niu, M.Q., Chen, L.Q., 2022. Tunable roton-like dispersion relation with parametric excitations. J. Appl. Mech. 89, 111005.
Duan, Z., Cui, J., Chen, L.Q., Yang, T., 2023. Nonlinear mechanical roton. J. Appl. Mech. 90, 31010.
Eringen, A.C., 1966. Linear theory of micropolar elasticity. Journal of Mathematics and Mechanics 15 (6), 909–923.
Fleury, R., 2021. Non-local oddities. Nat. Phys. 17 (7), 766–767.
Godfrin, H., Meschke, M., Lauter, H.J., Sultan, A., et al., 2012. Observation of a roton collective mode in a two-dimensional fermi liquid. Nature 483 (7391), 576–579.
Groß, M.F., Schneider, J.L.G., Chen, Y., Kadic, M., Wegener, M., 2024. Dispersion engineering by hybridizing the back-folded soft mode of monomode elastic metamaterials with stiff acoustic modes. Adv. Mater. 36 (6), 2307553.
Han, S., Li, C., Han, Q., Yao, X., 2025. Machine learning-aided prediction and customization on mechanical response and wave attenuation of multifunctional kiri/origami metamaterials. Extreme Mechanics Letters 74, 102276.
Iglesias Martínez, J.A., Groß, M.F., Chen, Y., Frenzel, T., Laude, V., Kadic, M., Wegener, M., 2021. Experimental observation of roton-like dispersion relations in metamaterials. Sci. Adv. 7 (49), eabm2189.
Jiao, P., Mueller, J., Raney, J.R., (Rayne) Zheng, X., Alavi, A.H., 2023. Mechanical metamaterials and beyond. Nat. Commun. 14 (1), 6004.
Kadic, M., Milton, G.W., van Hecke, M., Wegener, M., 2019. 3D metamaterials. Nat Rev Phys 1 (3), 198–210.
Karpov, E.G., Rahman, K.A., 2025. Unitary mechanical metamaterials with embedded one-qubit logic. Extreme Mechanics Letters 77, 102330.
Kazemi, A., Deshmukh, K.J., Chen, F., Liu, Y., Deng, B., Fu, H.C., Wang, P., 2023. Drawing dispersion curves: band structure customization via nonlocal phononic crystals. Phys. Rev. Lett. 131 (17), 176101.
Kishine, J., Ovchinnikov, A.S., Tereshchenko, A.A., 2020. Chirality-induced phonon dispersion in a noncentrosymmetric micropolar crystal. Phys. Rev. Lett. 125 (24), 245302.
Krushynska, A.O., Torrent, D., Aragón, A.M., Ardito, R., et al., 2023. Emerging topics in nanophononics and elastic, acoustic, and mechanical metamaterials: an overview. Nanophotonics 12 (4), 659–686.
Landau, L., 1941. Theory of the superfluidity of Helium II. Phys. Rev. 60 (4), 356–358.
Marin, L., 2009. The minimal error method for the Cauchy problem in linear elasticity. Numerical implementation for two-dimensional homogeneous isotropic linear elasticity. Int. J. Solid Struct. 46 (5), 957–974.
Marin, L., Lesnic, D., 2004. The method of fundamental solutions for the Cauchy problem in two-dimensional linear elasticity. Int. J. Solid Struct. 41 (13), 3425–3438.
Martínez, J.A.I., Chen, Y., Wang, K., Wegener, M., 2025. Nonlocal conduction in a metawire. Adv. Mater.
Milton, G.W., 2002. The Theory of Composites; Cambridge Monographs on Applied and Computational Mathematics. Cambridge University Press, Cambridge.
Prodan, E. Pro E., 2006. Analytic structure of bloch functions for linear molecular chains. Phys. Rev. B 73 (3), 035128 dan. Analytic structure of Bloch functions for linear molecular chains. Phys. Rev. B (2006), 73 (3), 035128.
Puglisi, G., 2006. Hysteresis in multi-stable lattices with non-local interactions. J. Mech. Phys. Solid. 54 (10), 2060–2088.
Puglisi, G., 2007. Nucleation and phase propagation in a multistable lattice with weak nonlocal interactions. Continuum Mech. Thermodyn. 19 (5), 299–319.
Rajabpoor Alisepahi, A., Sarkar, S., Sun, K., Ma, J., 2023. Breakdown of conventional winding number calculation in one-dimensional lattices with interactions beyond nearest neighbors. Commun. Phys. 6 (1), 1–12.
Samak, M.M., Bilal, O.R., 2024. Evidence of zero group velocity at the lowest dispersion branch through local interactions. APL Mater. 12 (1), 011111.
Shaat, M., Ghavanloo, E., Fazelzadeh, S.A., 2020. Review on nonlocal continuum mechanics: physics, material applicability, and mathematics. Mech. Mater. 150, 103587.
Wang, K., Chen, Y., Kadic, M., Wang, C., Wegener, M., 2022. Nonlocal interaction engineering of 2D roton-like dispersion relations in acoustic and mechanical metamaterials. Commun Mater 3 (1), 1–11.
Yang, T., Duan, Z., Meng, X., Liu, S., Chen, L.Q., 2023. Roton-enabled mechanical diode at extremely low frequency. J. Appl. Mech. 91, 011010.
Zhu, Z., Gao, Z., Liu, G.-G., Ge, Y., et al., 2022. Observation of multiple rotons and multidirectional roton-like dispersion relations in acoustic metamaterials. New J. Phys. 24 (12), 123019.